AGU PUBLICATIONS

JGR

Journal of Geophysical Research: Atmospheres

RESEARCH ARTICLE
10.1002/2016JD025656

Key Points:
- Outflow related to intensity
- Outflow centered near 200 hPa
- Outflow between areas of maximum and minimum inertial stability

Correspondence to:
B. S. Barrett and E. R. Sanabia,
bbarrett@usna.edu;
sanabia@usna.edu

Citation:
Barrett, B. S., E. R. Sanabia, S. C. Reynolds, J. K. Stapleton, and A. L. Borrego (2016), Evolution of the upper tropospheric outflow in Hurricanes Iselle and Julio (2014) in the Navy Global Environmental Model (NAVGEM) analyses and in satellite and dropsonde observations, *J. Geophys. Res. Atmos.*, *121*, 13,273–13,286, doi:10.1002/2016JD025656.

Received 15 JUL 2016
Accepted 29 OCT 2016
Accepted article online 2 NOV 2016
Published online 22 NOV 2016

Evolution of the upper tropospheric outflow in Hurricanes Iselle and Julio (2014) in the Navy Global Environmental Model (NAVGEM) analyses and in satellite and dropsonde observations

Bradford S. Barrett[1], Elizabeth R. Sanabia[1], Sara C. Reynolds[1], Julie K. Stapleton[1], and Anthony L. Borrego[1]

[1]Oceanography Department, U.S. Naval Academy, Annapolis, Maryland, USA

Abstract Upper tropospheric outflow was examined during the life cycles of two hurricanes in the eastern and central Pacific Ocean. The outflow from Hurricanes Iselle and Julio was evaluated by using analyses from the Navy Global Environmental Model, which were very highly correlated with satellite atmospheric motion vector and NOAA G-IV dropsonde observations. A synoptic overview provided the environmental context for the life cycles of both tropical cyclones (TCs). Then, the outflow magnitude and direction within 6 radial degrees of each TC center were analyzed in relation to TC intensity, the synoptic environment, and inertial stability, with the following results. In both Iselle and Julio, the azimuthally averaged outflow magnitude was maximized initially more than 4 radial degrees from the center, and that maximum moved steadily inward during a 4 day intensification period and reached a position radially inward of 2° within 6 h of the time of maximum surface winds. Furthermore, the direction of the outflow in both TCs was related to the evolution of the large-scale upper tropospheric flow pattern, particularly the phasing of subtropical jet ridges and troughs moving eastward north of both TCs. Finally, outflow channels were consistently bounded by regions of lowest (highest) values of inertial stability counterclockwise (clockwise) from the maximum outflow azimuth, a pattern that persisted throughout the life cycles of both storms regardless of intensity, environmental flow, and the number and direction of outflow channels present.

1. Introduction

Upper tropospheric air moving radially outward, often anticyclonically, from the center of a tropical cyclone (TC) classically has been referred to as outflow. After decades of observational and modeling study, this outward moving, upper tropospheric air has been found to be critically related to both TC track and intensity. For example, TC motion is, in part, determined by the interaction between outflow, the environment away from the TC, and the baroclinic TC inner core [*Wu and Emanuel*, 1993; *Wu and Kurihara*, 1996; *Henderson et al*., 1999; *Ferreira and Schubert*, 1999; *Corbosiero and Molinari*, 2003; *Harr et al*., 2008]. Furthermore, expansion of TC outflow, including that which often occurs during the extratropical transition of a poleward moving TC, can have significant implications for not only track but also larger, regional-scale circulation, as the outflow causes the destruction of environmental potential vorticity (PV) downstream of the TC [*Bosart and Dean*, 1991; *Harr and Elsberry*, 2000; *Torn*, 2010; *Grams et al*., 2013; *Archambault et al*., 2013; *Torn et al*., 2015]. In addition to its relationship to TC track, many studies have revealed a complex relationship between outflow and TC intensity. At its most basic level, outflow carries high potential temperature air away from the TC convective core, where it is cooled by radiation, thus completing one branch of the TC Carnot cycle [*Emanuel*, 1986]. Generally, the more outflow a TC has, the stronger it is, and outflow can often be identified in conventional geostationary satellite imagery as a "fanning out" of the central dense overcast [e.g., *Molinari et al*., 2014]. However, questions remain, including where, both vertically and horizontally, outflow is the strongest and whether changes in outflow precede, follow, or occur concurrently with, changes in intensity. Areas of intense, focused outflow have often been referred to as "outflow channels" or "outflow jets" [*Merrill and Velden*, 1996; hereafter MV96]. A primary goal of this study is to better understand the relationships between outflow and TC intensity by examining properties of outflow over the life cycles of two TCs in the eastern and central Pacific Ocean, Hurricanes Iselle and Julio (2014) (Figure 1).

Part of the complex relationship between TC intensity and outflow stems from the nonlinear effects of inertial stability in the outflow layer. *Holland and Merrill* [1984] found that the upper troposphere–lower stratosphere

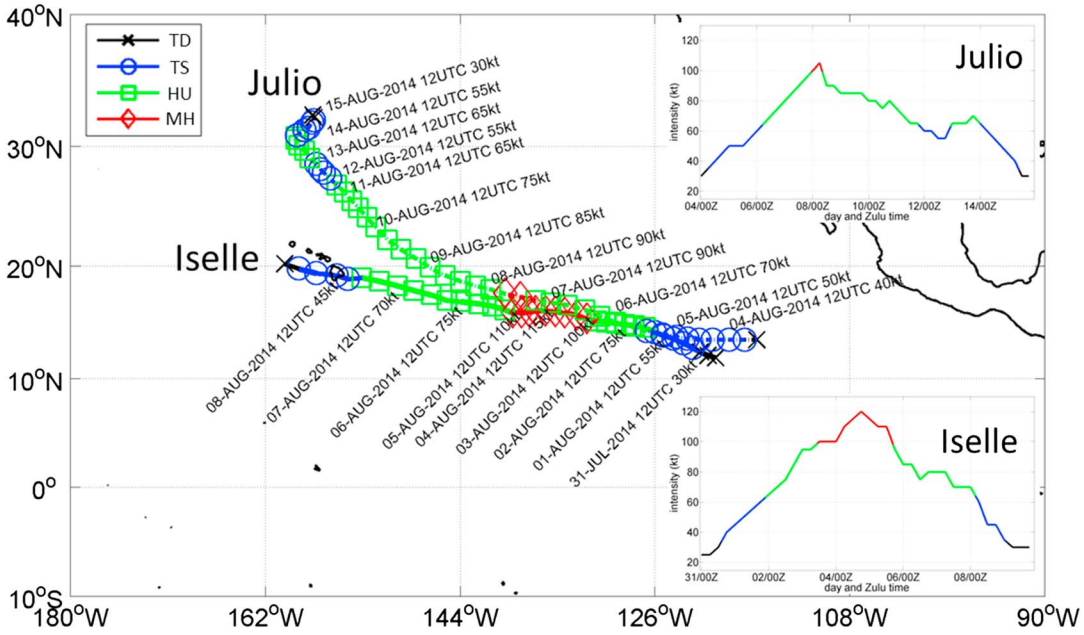

Figure 1. Tracks and intensities (insets) of Hurricanes Iselle (2014) and Julio (2014). Tropical depression intensity represented by black cross marks, tropical storm intensity by blue circles, hurricane intensity by green squares, and major hurricane intensity by red diamonds.

layer above a TC is susceptible to external forcing (such as from passing extratropical waves) due to the low inertial stability of the anticyclonic outflow. Therefore, asymmetries in the outflow layer (for example, a poleward outflow channel without a corresponding equatorward one) exist as a response of the TC outflow to external environmental features [*Holland and Merrill*, 1984; *Flatau and Stevens*, 1989; *Molinari et al*., 2014]. Sawyer-Eliassen balanced vortex dynamics dictate that the positive angular momentum source associated with the approach of an upper tropospheric trough will create an increase in TC outflow to mitigate an imbalance near the tropopause [*Montgomery and Smith*, 2014; *Peirano et al*., 2016]. *Rappin et al*. [2011] found that the formation of a channel of outflow was a response to TC outflow expanding into a region of weak inertial stability on the anticyclonic shear side of a jet stream and that connection between TC outflow and the inertial stability of the environment was also found by *Sears and Velden* [2014]. When this outflow ventilation was concentrated in one narrow, long channel, the least energy expenditure was required [*Rappin et al*., 2011]. Indeed, these channels can be the result of coupling between the TC anticyclonic outflow and an approaching cold-core upper tropospheric trough, including through thermal wind balance [*Molinari and Vollaro*, 1989]. The coupling of outflow jet streaks between TCs and troughs was identified in composite analyses of TCs from the 1980s and early 1990s as being favorable for TC intensification, a process sometimes referred to as a "good trough" interaction [*Hanley et al*., 2001].

Other studies have found that both the total amount of convection and the intensity of the TC surface winds appear to be affected by interactions between the storm and external circulations. For example, *Molinari et al*. [1995] showed that upper level PV anomalies, such as those associated with upper level troughs, can either weaken a tropical cyclone by increasing vertical shear over the core or intensify it by unbalancing the upper level flow leading to enhanced divergence of mass from the core (hence increasing the total convection). *Merrill* [1988] found that intensifying TCs exhibit asymmetric patterns in their outflow, including outflow organized into one or more outflow channels, and *Pfeffer and Challa* [1992] and *Frank and Ritchie* [1999] confirmed that enhanced upper level outflow favors storm intensification. Outflow channels can form in response to the relatively strong temperature gradient between the warmer TC and the colder extratropical trough [*Molinari et al*., 2014].

Connecting outflow to intensity, *Merrill and Velden* [1996] found that for Supertyphoon Flo (1990), at a radius of 6° (about 600 km) from the storm center, the stronger the typhoon was, the higher (vertically) the outflow was found. Furthermore, they found that outflow on the equatorward side of Flo tended to be located at higher altitudes (greater potential temperature values) than the poleward outflow. In part, because of

uncertain interaction they found between Flo and a tropical upper troposphere trough feature, MV96 encouraged future studies on outflow—particularly emphasizing studies that examine the temporal evolution and vertical structure of outflow—be undertaken to add to the conceptual models of TC-environment interaction. They acknowledged that because outflow is associated with a negative PV anomaly, the presence of outflow and outflow jets at different altitudes over the life cycle of the storm is likely to evolve nonlinearly with TC intensity. *Emanuel and Rotunno* [2011] revisited some of the questions raised by MV96 from a theoretical perspective and found that the majority of outflow was located below the tropopause. *Molinari et al*. [2014] also revisited some of the questions raised by MV96, using dropsonde observations in Hurricane Ivan (2004). They found that outflow reached a maximum near 12 km altitude around 500 km from the storm center, and the largest amount of turbulence, and vertical shear of the horizontal wind, was found at a mean height of 13 km [*Molinari et al*., 2014]. Furthermore, other recent studies have returned to focus on upper tropospheric/lower stratospheric outflow, finding that outflow serves as a major control on TC potential intensity [*Rotunno and Emanuel*, 1987; *Emanuel*, 2010; *Mrowiec et al*., 2011; *Emanuel and Rotunno*, 2011; *Ramsay*, 2013; *Chavas and Emanuel*, 2014), including on interannual and longer time scales [*Emanuel et al*., 2013].

Given these observational and theoretical results, it is clear that upper tropospheric outflow, together with moist convection in the TC core, provides a critical connection between the near-storm upper tropospheric environment and the TC boundary layer [*Emanuel*, 2012; *Wang et al*., 2014]. Thus, one purpose of this study is to improve understanding of TC outflow, including its magnitude and direction and relationship to inertial stability, with particular focus on how changes in outflow intensity and position may coincide with changes in TC intensity at the surface. Here we seek to build on observational outflow studies such as *Molinari et al*. [2014] and *Molinari and Vollaro* [2014], theoretical outflow studies such as *Emanuel and Rotunno* [2011] and *Emanuel* [2012], and modeling outflow studies such as *Wang et al*. [2014] by using observations coupled with 6 h high-resolution gridded analyses from the Navy Global Environmental Model (NAVGEM) [*Hogan et al*., 2014] to describe the evolution of outflow during the life cycles of two hurricanes.

The remainder of this paper is organized as follows: data and methods are presented in section 2, followed by a description of the synoptic life cycle of both Hurricanes Iselle and Julio (2014) in section 3. In section 4, the evolution of outflow over the life cycles of both TCs is presented and the inertial stability in the vicinity of each TC is analyzed. Conclusions and discussion are presented in section 5.

2. Data, Methods, and Data Quality

2.1. Data and Methods

Gridded model analyses of *u* and *v* wind components were taken from NAVGEM analyses (available at http://www.usgodae.org/) at nine pressure levels (1000 hPa, 850 hPa, 700 hPa, 500 hPa, 300 hPa, 250 hPa, 200 hPa, 150 hPa, and 100 hPa) at 6 h intervals from 0000 UTC on 31 July 2014 to 0000 UTC on 16 August 2014, spanning the entire life cycles of Hurricanes Iselle and Julio (2014). Analyses from the NAVGEM model were used instead of reanalyses to take advantage of higher horizontal-resolution gridded data (NAVGEM analyses are available at 0.5° horizontal resolution). For each analysis of time and pressure level, the storm center was manually located by subjectively identifying the best co-location of minimum wind speed and circulation center. The manual storm-center identification method was used instead of relying on NOAA National Hurricane Center and Central Pacific Hurricane Center center positions because of potential position mismatches between the observed TC and the NAVGEM analyses and to account for potential vortex tilt with height. Once center locations were identified, Cartesian *u* and *v* wind components were transformed into polar u_r and u_θ wind components, with positive u_r indicating flow radially outward from the TC, negative u_r indicating flow radially inward toward the TC center, and positive u_θ corresponding to counterclockwise azimuthal flow. Azimuthal u_θ wind components were used to calculate inertial stability. This study only focused on outflow that was radially inward of 6° from the storm center, most directly following the choice of 600 km by MV96 and *Molinari and Vollaro* [2014]. That limit was set to isolate outflow that was connected to processes in the TC inner core. The choice of 6° also was similar to other work on TC outflow [e.g., *Black and Anthes*, 1971; *Franklin et al*., 1993; *Rappin et al*., 2011].

One of the concerns with using NAVGEM model output to diagnose outflow from Iselle and Julio was that the model may not have accurately captured upper level winds, and thus could have misrepresented the outflow. To test this hypothesis, atmospheric motion vectors (AMVs, available at http://tropic.ssec.wisc.edu/archive/)

from geostationary satellite observations within 1 h of NAVGEM analysis times were compared to NAVGEM wind speed and u_r calculations. The AMVs are observations of wind speed and direction generated by tracking water vapor features, or clouds, in consecutive satellite images. The tracked features are assumed to act as passive tracers of the atmospheric flow. During the AMV calculation, a representative pressure level, estimated either as cloud base or top, is assigned. The AMVs have global coverage at the spatial and temporal resolutions of the parent satellite and are particularly useful over the open ocean where other observations are scarce. Additional information on AMVs and their potential errors can be found in *Salonen et al*. [2015], *Velden et al*. [2005], *Menzel* [2001], *Nieman et al*. [1997], and *Schmetz et al*. [1993]. Information on the assimilation of AMV observations into global and regional modeling systems can be found in *Bormann et al*. [2012], *Cotton and Forsythe* [2012], *Cress* [2012], *Pauley et al*. [2012], and *Su et al*. [2012].

Observations from GPS dropsondes released during NOAA G-IV synoptic surveillance flights were also used to examine how well NAVGEM output represented the outflow. The GPS dropsonde data were obtained from the NOAA Atlantic Oceanographic and Atmospheric Laboratory (AOML) Hurricane Research Division (available at http://www.aoml.noaa.gov/hrd/Storm_pages/iselle2014/mission.html). To best match with NAVGEM values, dropsonde data were restricted to within 1 h of synoptic time (0000, 0600, 1200, or 1800 UTC). The four NOAA G-IV flights occurred between 05 and 09 August 2014. At the level with consistently strongest outflow (200 hPa), 39 dropsonde observations were retained and compared to NAVGEM values.

It is possible, even likely, that the NAVGEM model analyses included many, if not most, of the AMV and dropsonde observations (and as shown in section 2.2, correlations between NAVGEM and AMV, and NAVGEM and dropsonde, observations were high to very high). In the absence of this comparison to satellite and GPS dropsonde observations, confidence in the NAVGEM to represent the wind field both near (within 6°) and far (outside of 6°) from the TC centers would have been comparatively less.

2.2. Data Quality

To provide confidence in the NAVGEM model outflow analyses described in section 2.1, 200 hPa winds in the NAVGEM were compared to 200 hPa winds in two observational data sets: the cloud-track AMV winds and the dropsonde observations made by the NOAA synoptic surveillance G-IV aircraft. Satellite observations were available between 0000 UTC on 01 August 2014 and 1800 UTC on 15 August 2014, a period covering the life cycles of both Iselle and Julio, while dropsonde observations were available between 1800 UTC on 05 and 09 August 2014 (a period when both Iselle and Julio threatened Hawaii and thus were sampled by reconnaissance aircraft). Differences in speed between satellite AMV and model NAVGEM winds at 200 hPa ranged from $-10\,\mathrm{m\,s^{-1}}$ to $10\,\mathrm{m\,s^{-1}}$, but the majority of observations had speed differences less than $\pm 2\,\mathrm{m\,s^{-1}}$ (Figure 2). Wind speed differences showed neither an obvious cluster or pattern association (e.g., wind speed differences did not cluster by magnitude around the synoptic-scale trough-ridge features or near particular latitude or longitude bands) nor were there clear differences for weak or strong winds. Given the agreement between the model and the observations, confidence in the subsequent outflow analysis based on NAVGEM is strengthened.

In addition to overall wind speed, the radial and azimuthal wind components were calculated for the AMV and dropsonde observations—and the positive radial components were analyzed. The radial wind components in both NAVGEM analyses and AMVs were strongly positively correlated (Pearson product-moment correlation coefficients of 0.94 for Iselle and 0.91 for Julio) with biases around $0.4\,\mathrm{m\,s^{-1}}$ for Iselle and $-1.0\,\mathrm{m\,s^{-1}}$ for Julio (Figure 3a). These biases and correlations were based on 1299 and 2010 observation comparisons for Iselle and Julio, respectively. Correlations between NOAA G-IV dropsonde outflow and NAVGEM outflow were even higher: for the 76 total dropsonde observations in both TCs, the Pearson correlation coefficient was 0.96, with a bias of only $0.46\,\mathrm{m\,s^{-1}}$ (Figure 3b). Correlations and biases for each individual storm were very similar: correlation of 0.96, bias of $0.27\,\mathrm{m\,s^{-1}}$, for Iselle (37 observations), and correlation of 0.96, bias of $0.64\,\mathrm{m\,s^{-1}}$, for Julio (39 observations). Given the high correlations between NAVGEM and both AMV and dropsonde winds, it is likely that some, or even most, of the observational data were assimilated into the NAVGEM model and thus were included in the 0 h analyses used in this study. However, the objective of the study was to use the NAVGEM data to explore outflow, and thus, the high correlations with observational data give confidence in the model representation of outflow at the 200 hPa level.

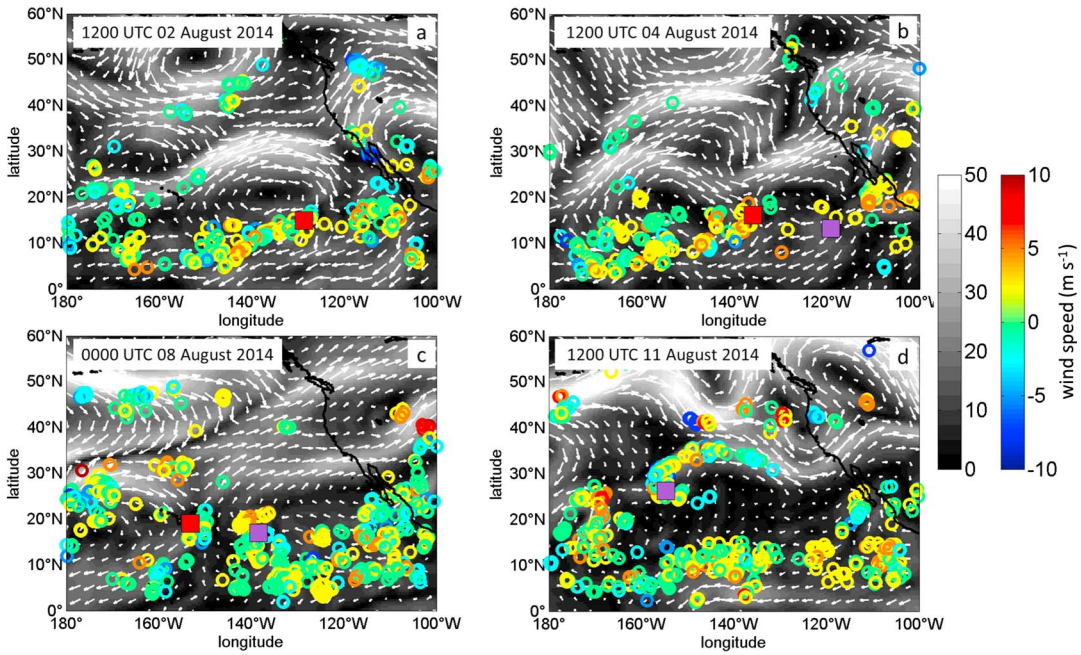

Figure 2. The NAVGEM 200 hPa wind speeds (gray shading, in m s^{-1}) and vectors (white arrows) for (a) 1200 UTC on 02 August 2014, (b) 1200 UTC on 04 August 2014, (c) 0000 UTC on 08 August 2014, and (d) 1200 UTC on 11 August 2014. The colored squares indicate the positions of Iselle (red) and Julio (purple). The colored circles indicate wind speed differences (m s^{-1}) between NAVGEM output and AMV observations, and the colored triangles indicate wind speed differences (m s^{-1}) between NAVGEM output and NOAA G-IV dropsonde observations (scale at right).

3. Hurricanes Iselle and Julio (2014): Life Cycle Summaries and Synoptic Overview

Hurricanes Iselle and Julio formed in the eastern North Pacific within 4 days and 525 km of each other. Iselle first reached tropical storm (TS) intensity at 12.8°N, 122.5°W at 1800 UTC on 31 July 2014 [*Kimberlain*, 2014] and tracked west-northwestward toward the Big Island of Hawaii (Figure 1). Julio first reached TS intensity shortly thereafter, at 13.5°N, 117.7°W at 0600 UTC on 04 August 2014 [*Stewart*, 2015], and followed westward in the wake of Iselle (Figure 1). Both TCs reached Category 3 intensity while tracking west-northwestward beneath a subtropical ridge located over the eastern Pacific Ocean. While Iselle remained on a predominantly westward track and decayed following landfall on the Big Island of Hawaii on 08 August 2014, Julio tracked consistently northwestward, passing east of the Big Island before reintensifying

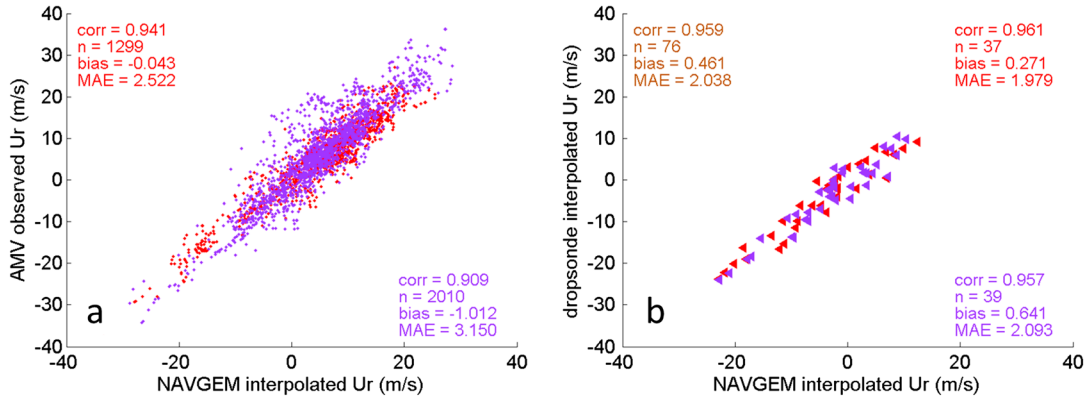

Figure 3. Outflow comparison of 200 hPa NAVGEM to (a) AMV and (b) dropdsonde outflow magnitudes at AMV locations within 6° of the TC center (Figure 3a) and all dropsonde locations (Figure 3b). The red colors correspond to Hurricane Iselle, and the purple to Hurricane Julio. Pearson-product correlation coefficients (corr), sample size (*n*), bias (NAVGEM minus observation), and mean absolute error (MAE) provided for each storm (red and purple colors in Figures 3a and 3b) and together (brown color in Figure 3b).

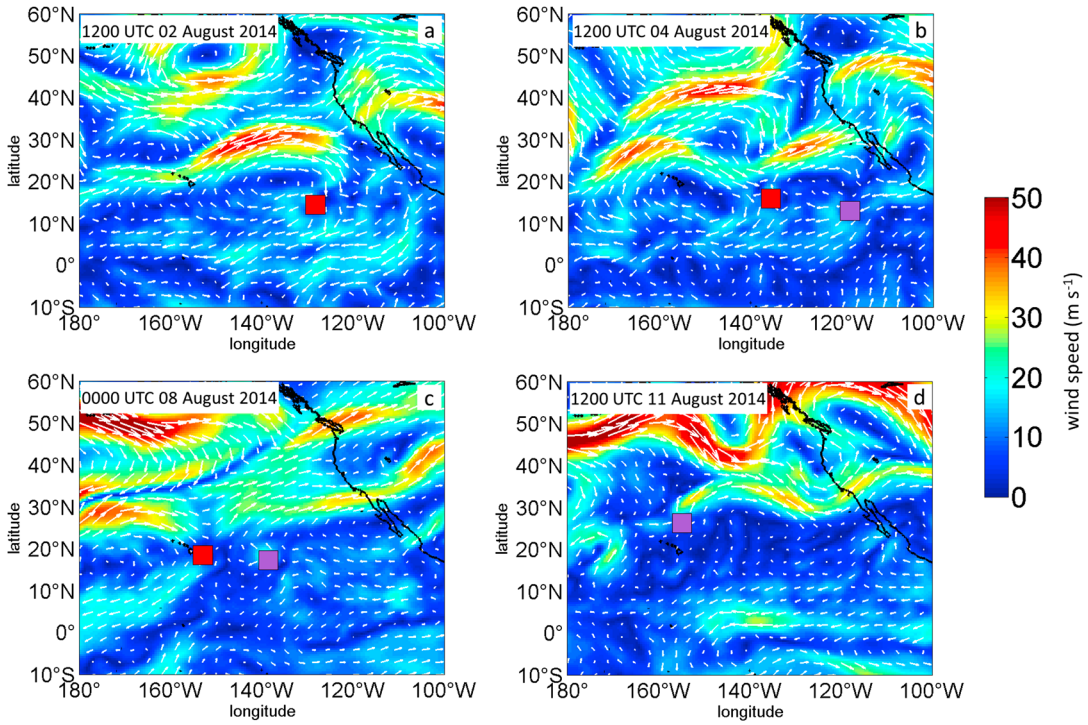

Figure 4. Wind speeds (shaded, in m s^{-1}) and vectors (white arrows) at 200 hPa in the NAVGEM model. The dots indicate positions of Hurricane Iselle (red) and Hurricane Julio (purple) at the times in Figure 2. Only Iselle is present in Figure 4a, and only Julio is present in Figure 4d.

to hurricane intensity at 0000 UTC on 13 August 2014 more than 1000 km north of Lihue, HI. Julio remained at hurricane intensity for 30 h, then turned northeastward and decayed below TS intensity near 32.3°N, 157.5°E at 1200 UTC on 15 August 2014.

The synoptic situation over the tropical eastern Pacific Ocean during the life cycles of Iselle and Julio was dominated by a ridge-trough-ridge pattern within the subtropical jet. At 1200 UTC on 02 August 2014 (Figure 4a), Iselle (maximum surface wind of 75 kt) was located just south of the leading edge of the subtropical ridge. Northerly flow from this ridge contributed to a predominantly equatorward flow away from Iselle (Figure 4a, white arrows). The ridge moved east as Iselle moved west.

By 1200 UTC on 04 August 2014 (Figure 4b), Iselle (maximum surface wind of 115 kt) was located at the ridge's western (trailing) edge and to the southeast of a trough with its axis near 145°W. Synoptic-scale flow was northward away from the TC and into the entrance region of a jet streak within the ridge to the northeast of Iselle. To the west of Iselle, another anticyclone was centered near 150°W. To the east of Iselle, recently formed Julio (maximum surface wind of 40 kt) was located to the southeast of the ridge (Figure 4b).

On 0000 UTC on 08 August 2014 (Figure 4c), as Iselle (maximum surface winds of 70 kt) made landfall, a ridge northwest of Hawaii resulted in synoptic-scale northwesterly flow impinging on the northern circulation of Iselle. To the east, the synoptic-scale flow was away from Julio (maximum surface winds of 100 kt) and into the eastern edge of a trough to the northwest of the TC (Figure 4c). Julio continued to move westward then northward to the west of a ridge axis centered near 140°W (Figure 4d). By 1200 UTC on 11 August 2014 (Figure 4d), Julio (maximum surface winds of 65 kt) was south of the western edge of this ridge, and synoptic-scale flow over Julio was northward and northeastward.

These four synoptic snapshots into the life cycles of Iselle and Julio provide details of the evolution of the larger-scale environmental flow through which both TCs transited. Within this synoptic-scale framework, the evolution of the TC outflow in closer proximity to the TC is examined in greater detail in the next section, with particular focus on outflow structure and relationships to TC intensity and inertial stability.

4. Outflow Evolution in the NAVGEM Analyses

4.1. Outflow Analysis

One of the first questions regarding outflow evolution during Iselle and Julio was where, vertically, the outflow was located. As noted in the methodology, to isolate outflow only positive values of radial flow (u_r) were used. Azimuthally averaged outflow was then calculated at 0.5° increments radially outward to 6° from the TC center at standard pressure levels for each analysis time (Figures 5d and 5e). Largest average outflow magnitudes were found between 150 and 200 hPa (vertically) and between 2 and 5 radial degrees from the TC center (horizontally) for both storms. Locations of greatest outflow at each time step in the storms' life cycles are given as gray symbols, with circles indicating the radial and vertical positions of largest outflow magnitude for each 6 h NAVGEM analysis when the TC was at tropical storm intensity (35–60 kt), triangles during hurricane intensity (65–95 kt), and squares during major hurricane intensity (100+ kt). For both Iselle and Julio, largest outflow magnitudes were most frequently located at 200 hPa and were always found between 250 hPa and 100 hPa. Because of this clustering at 200 hPa, outflow at 200 hPa was selected for the remainder of the analysis.

In section 3, the evolution of Iselle and Julio within the larger-scale environmental flow was discussed at four representative time steps. Here the focus is on the evolution of the outflow at 200 hPa closer to the storm, within 6° latitude and longitude of the TC center, at the same times as in the analysis above. At 1200 UTC on 02 August 2014 (Figure 5a), positive radial flow up to 20 m s^{-1} was evident southwest of Iselle, while negative radial flow (inflow) was present to a lesser extent in the northeast quadrant, with speeds to −15 m s^{-1}. This outflow pattern corresponded to the position of Iselle southeast of a ridge in the subtropical jet at that time (Figure 4a). At 1200 UTC on 04 August 2014 (Figure 5b), dual outflow channels were present, one to the north of Iselle and another to the south, with radial flow again approaching 20 m s^{-1}. This outflow pattern also agreed with the synoptic-scale flow in Figure 4b, where Iselle was located southeast of the trough axis. With the approach of an upper tropospheric ridge at 0000 UTC on 08 August 2014 (Figure 5c), strong inflow, near −25 m s^{-1}, approached Iselle from the northwest, while the strongest outflow, near 25 m s^{-1}, remained focused southwest of the TC. There was still outflow present northeast of Iselle toward the trough and jet.

At 1200 UTC on 04 August 2014 near the start of the life cycle of Julio, 200 hPa flow was mostly northeasterly (Figure 4b), resulting in mostly inflow into Julio (around −10 m s^{-1}) in the northeastern quadrant and outflow (around 10 m s^{-1}) in the western quadrants (Figure 5f). By 0000 UTC on 08 August 2014 (Figure 5g), outflow (up to 15 m s^{-1}) was present in all quadrants of Julio, but the dominant outflow was located northwest of the TC toward the trailing edge of the subtropical ridge (Figure 4c). At 1200 UTC on 11 August 2014, outflow up to 25 m s^{-1} was located northeast of Julio (Figure 5h), in connection with the upper level trough (Figure 4d), while inflow around −5 m s^{-1} was located to the south of Julio. In both TCs, the meridional orientation of the outflow was consistent with the phasing of the subtropical jet; i.e., equatorward (poleward) directed outflow generally occurred when the TC was southeast (southwest) of the ridge axis.

4.2. Hovmoller Analysis

Analyzing Hovmoller diagrams of azimuthally averaged outflow (Figure 6) provides additional insight into the spatial and temporal evolution of the outflow from both Iselle and Julio during their respective life cycles. In Hurricane Iselle, there was a clear difference in azimuthally averaged 200 hPa outflow magnitude over approximately the first and second halves of the TC life cycle (Figure 6a). For the first half (between 1200 UTC on 31 July 2014 and 0000 UTC on 06 August 2014; Figure 6a), a broadband of outflow, with azimuthal mean values in excess of 5 m s^{-1}, was found within 6° of Iselle's center. Also, during that time frame, the position of the 7 m s^{-1} isotach gradually progressed radially inward, from nearly 4° away from Iselle's center at 1200 UTC on 31 July 2014 to less than 2° away from Iselle's center at 0000 UTC on 05 August 2014. During this 108 h radially inward shift in maximum outflow magnitude, Iselle intensified more than 80 kt and reached maximum intensity just 6 h before the maximum outflow was located closest to the TC center. As the maximum outflow slowly shifted radially outward on 05 August 2014, Iselle's surface winds began to weaken. The TC continued to weaken during the second half of its life cycle, during which the outflow magnitude decreased below 4 m s^{-1}. This period of weaker outflow occurred as Iselle passed west of the trough axis and south of an anticyclonic wave-breaking event (Figure 4c). Outflow during the TC's final 3 days was fairly evenly distributed from near Iselle's center radially outward to 6° from the center and was weakest on 08 August 2014 following landfall on the Big Island.

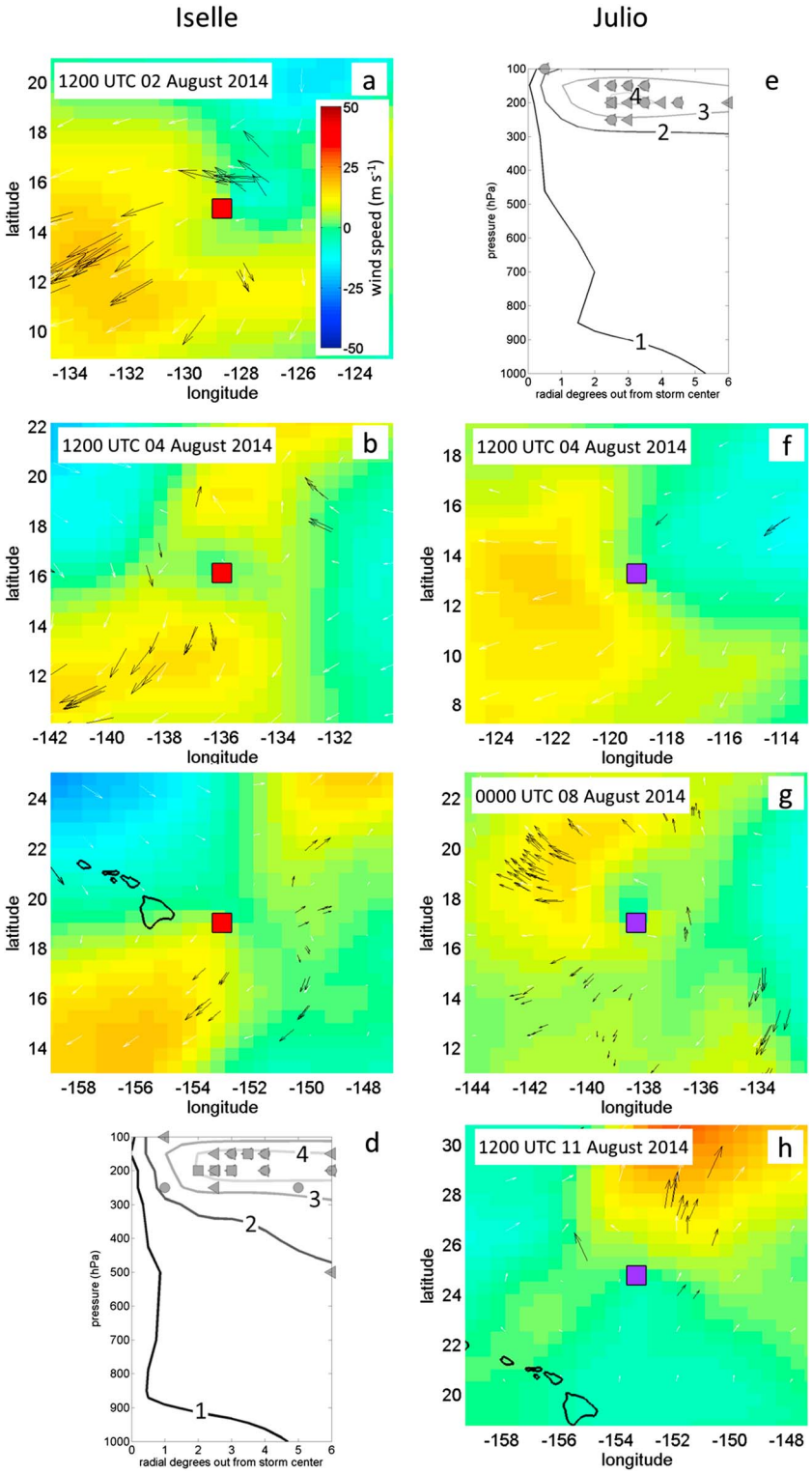

Figure 5. Storm-relative outflow at 200 hPa (shaded, speeds in m s^{-1}) for (a–c) Iselle and (f–h) Julio for the synoptic times in Figure 2. The colored squares indicate center positions for Iselle (red) and Julio (purple). The white arrows indicate the 200 hPa total wind (as in Figure 2). The black arrows indicate satellite atmospheric motion vector (AMV) observations at 200 hPa within 1 h of the synoptic time. Azimuthally averaged outflow (m s^{-1}) over the entire life cycle is presented for (d) Iselle and (e) Julio. The gray symbols in Figures 5d and 5e indicate positions (radial and vertical) of greatest outflow magnitude at 6 h intervals, with tropical storm intensity indicated by gray circles, hurricane intensity by triangles, and major hurricane intensity by squares.

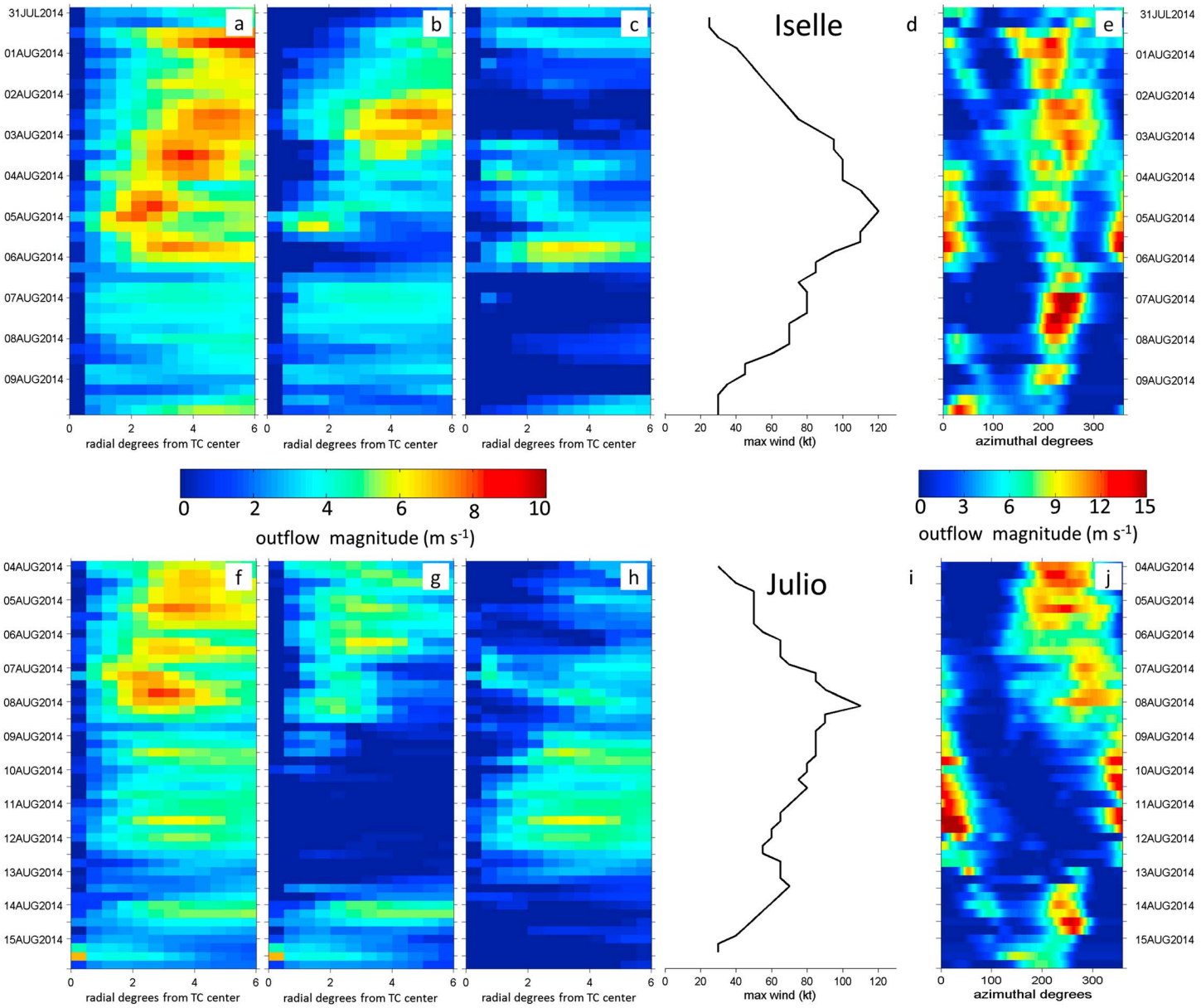

Figure 6. Hovmollers of azimuthally averaged positive outflow, equatorward outflow, and poleward outflow for (a–c) Iselle and (f–h) Julio (speeds in $m\,s^{-1}$). Intensities of (d) Iselle and (i) Julio over time. Hovmollers of radially averaged outflow for (e) Iselle and (j) Julio (speeds also in $m\,s^{-1}$ and north is 0°).

Stratification of the outflow into equatorward (southward; Figure 6b) and poleward (northward; Figure 6c) components revealed the meridional variation in outflow. On 31 July 2014 Iselle was at tropical storm intensity, and weak outflow extended both equatorward (at $4\,m\,s^{-1}$ starting around 3° from the center) and poleward (at $3\,m\,s^{-1}$ starting around 1° from the center). Two days later, equatorward outflow at 200 hPa increased markedly, to azimuthal mean values over $7\,m\,s^{-1}$, particularly 3–5° from the TC center, while the poleward outflow component decreased to nearly zero. This strong equatorward outflow continued for 24 h, and then weakened (Figure 6b) as the poleward component reintensified (Figure 6c). Between 03 and 05 August 2014, azimuthal mean outflow of over $4\,m\,s^{-1}$ extended both equatorward and poleward (Figure 5b). Also, during that time, Iselle's maximum surface winds increased by 25 kt and reached a maximum intensity of 120 kt at 1800 UTC on 04 August 2014 (Figure 6d). The dual channels persisted until 1200 UTC on 05 August 2014, when nearly all outflow was directed poleward and was maximized

2–5° from the TC center. Then somewhat abruptly, at 0000 UTC on 06 August 2014, the poleward outflow component mostly disappeared, while weak (less than 4 m s^{-1}) equatorward outflow dominated. This shift coincided with anticyclonic wave breaking in the ridge to the north of Iselle.

While the meridional velocity component identifies equatorward or poleward outflow (Figures 6b and 6c), another important factor to consider is the azimuth(s) along which most outflow is focused, since this location will identify the position(s) of the outflow channel(s). To locate these positions, radially averaged outflow is analyzed over time by using an azimuthal Hovmoller plot (Figure 6e). For Iselle, the 200 hPa radially averaged outflow out to 6° from the storm center was greatest at two locations around the TC center. One channel was consistently focused southwest of the TC, between about 190° and 270° (Figure 4e). A second channel was evident for about 48 h from 03–05 August 2014 on the north side of the TC, between about 340° and 040° (Figure 4e). The presence of this dual outflow channel configuration was noted previously (Figure 5c). Outflow magnitude in both these channels frequently averaged 12 m s^{-1}; however, on 05 August 2014, magnitude in the southern (equatorward outflow) channel decreased to about 8 m s^{-1}, while outflow in the northern (poleward outflow) channel exceeded 15 m s^{-1} (Figures 4b and 4c). While dual outflow channels were present at the time of maximum intensity (1800 UTC on 04 August 2014; Figure 4d), they were also present as the TC began to decay (on 05 August 2014).

Outflow during the life cycle of Julio exhibited several patterns similar to those observed during Iselle. For example, outflow magnitude was greatest (at or above 7 m s^{-1}), during the intensification phase of Julio (between 04 and 08 August 2014; Figure 6i) and weakest during the decay phase. The maximum outflow also progressed radially inward (Figure 6f) during the 4 day period as Julio's intensity increased by 75 kt. It is also clear that, like Iselle, the majority of outflow was directed equatorward (Figure 6g) during most of the intensification period and that at peak intensity (105 kt at 0000 UTC on 08 August 2014; Figure 6i), outflow was present briefly in both the equatorward and poleward directions, from about 1–3 and 3–6 radial degrees from the TC center, respectively (Figures 6g and 6h). As in Iselle, a weakening in outflow magnitude (Figure 6f) followed maximum intensity, and Julio continued to decay as outflow shifted meridional orientation from primarily equatorward to primarily poleward (Figures 6g and 6h). Poleward outflow, directed into the subtropical ridge, persisted for more than 3 days as the TC moved northwestward (Figure 5h).

Toward the end of Julio's life cycle, the TC briefly reintensified to hurricane strength (Figure 6i) and that reintensification was associated with a weakening of the poleward directed outflow (Figure 6g). The TC then decayed as outflow shifted equatorward (Figure 6h). Also, unlike Iselle, where two outflow channels remained somewhat constrained azimuthally to the south and north sides of the TC center (Figure 6e), outflow in Julio remained in a single channel that rotated anticyclonically around the TC center (Figure 6j).

4.3. Inertial Stability

In addition to the relationship between outflow and maximum surface winds presented above, outflow was also found to be related to inertial stability, I^2. Here I^2 was calculated at 200 hPa for each storm from the gridded NAVGEM wind fields at 6 h time steps from 31 July 2014 to 15 August 2014 as

$$I^2 = (\zeta + f_0)\left(f_0 + \frac{2V_\theta}{r}\right) \tag{1}$$

where ζ represents the relative vorticity, f_0 represents the Coriolis parameter on an *f*-plane tangent to the Earth at the TC near-surface (850 hPa) center, V_θ represents the 200 hPa azimuthal wind, and r represents the radial distance from the near-surface center [e.g., *Shapiro and Montgomery*, 1993]. Increased inertial stability creates resistance to outflow [*Schubert and Hack*, 1982; *Shapiro and Willoughby*, 1982; *Hack and Schubert*, 1986], and the formulation of I^2 follows the methodology of *Rappin et al.* [2011] and *Rozoff et al.* [2012]. Hovmoller diagrams of radially averaged I^2 show that for both Iselle and Julio, highest values of outflow were generally located clockwise (counterclockwise) from the lowest (highest) values of I^2 (Figure 7). For example, for Iselle, from 31 July 2014 to 04 August 2014, greatest outflow was located between 180 and 250° (e.g., outflow to the south and southwest; outflow shaded in Figure 5e and contoured in Figure 7a), while lowest I^2 was located between 130 and 200° (shaded in Figure 7a). Highest I^2 was located between 270 and 360° (shaded in Figure 7a). Even when Iselle featured two outflow channels on 04 and 05 August 2014, regions of lowest (highest) I^2 were consistently located counterclockwise (clockwise) from each outflow channel. This spatial pattern also was observed in Julio. From 04 to 07 August, while greatest outflow was located between 180 and 310° (shaded in

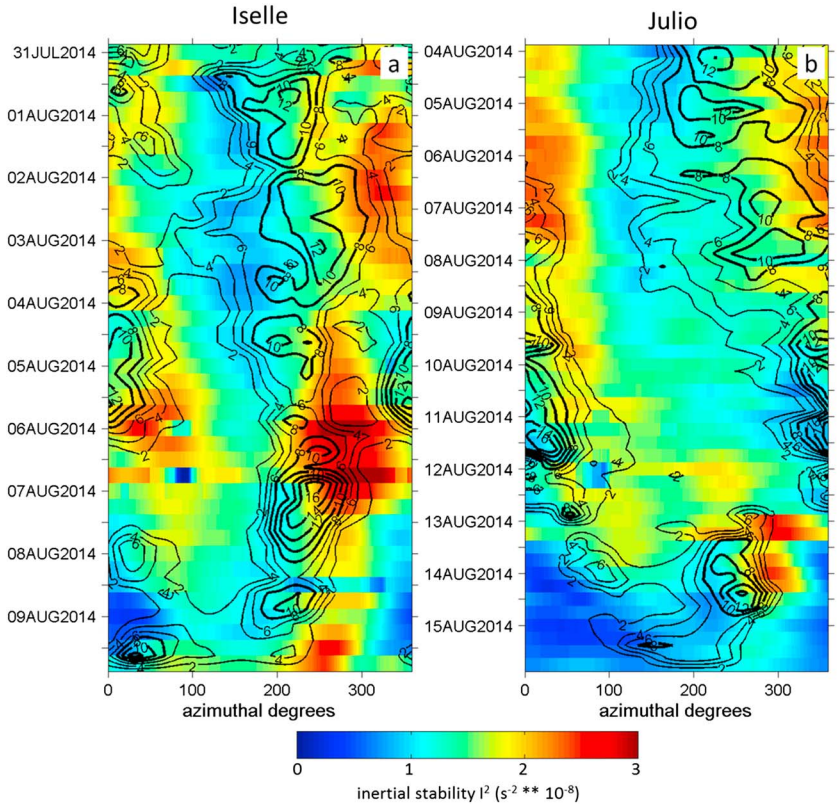

Figure 7. Hovmollers of radially averaged inertial stability (I^2 shaded, in s^{-2} ** 10^{-8}) and outflow (black contours, in m s^{-1}) averaged from the tropical cyclone center out 6° (approximately 600 km) for (a) Iselle and (b) Julio (north is 0°).

Figure 6j and contoured in Figure 7b), lowest I^2 was located between 130 and 180° (shaded in Figure 7b) and highest I^2 was located between 310 and 60° (shaded in Figure 7b). As the outflow in Julio evolved clockwise from primarily northeasterly (04 to 08 August 2014) to primarily southerly (10 to 12 August 2014), minimum I^2 also shifted clockwise, maintaining a similar offset between outflow and I^2 to that observed in Iselle. These spatial offsets between outflow and inertial stability in both Iselle and Julio extend the results of *Rappin et al.* [2011], who found that areas of reduced inertial stability (i.e., on the anticyclonic shear side of a midlatitude jet) were favored locations for TC outflow channels. Here the azimuthal orientation of the inertial stability was found to be consistent, relative to the outflow. Outflow channels were consistently bounded by regions of lowest (highest) values of inertial stability counterclockwise (clockwise) from the maximum outflow azimuth, a pattern that persisted throughout the life cycles of both storms regardless of intensity, environmental flow, and the number and direction of outflow channels present. A conceptual framework for this inertial stability distribution across the outflow channel is presented in Figure 8.

The presence of inertial stability maxima (minima) clockwise (counterclockwise) from the outflow maximum may be surprising at first, particularly when considering that the values of relative vorticity are a minimum (maximum) at those locations, due to the presence of cyclonic (anticyclonic) shear (Figure 8). Assumption of an *f* plane and use of a radial average mean that both f_0 and r will be identical on either side of the outflow jet. The remaining variable in equation (1) is the azimuthal wind, and it is the variation in that variable across the outflow channel that leads to the I^2 pattern exhibited in the cases of Iselle and Julio (Figure 7). In each case, anticyclonic outflow will exhibit a smaller (larger) azimuthal velocity component counterclockwise (clockwise) from the outflow jet (Figure 8). Depending on the jet orientation, the V_θ value clockwise from the jet may be a small positive or small negative value; however, for anticyclonic outflow, it will always be larger than the azimuthal outflow component on the counterclockwise side (Figure 8). Physically, this result means that a TC's outflow can affect the environmental inertial stability, as the orientation of an outflow jet can modify the sign and magnitude of relative vorticity and azimuthal velocity.

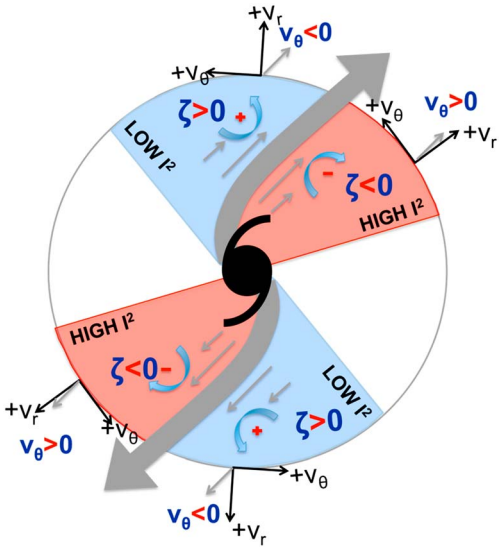

Figure 8. Conceptual schematic detailing regions of lower (higher) inertial stability counterclockwise (clockwise) from outflow channels with supporting mathematics. The color shadings (blue and red) were selected to correspond with lower (indicated by cooler colors) and higher (indicated by warmer colors) inertial stability in Figure 7.

Finally, while it is recognized that outflow can extend well beyond the 6 radial degrees from the TC center analyzed in this study, the relative values of ζ and V_θ should remain consistent across the outflow channel, even at extended radii. Noting that the orientation of the inertial stability maximum and minimum in this study were present in both Iselle and Julio at nearly every time step revealed an insensitivity of the distribution of inertial stability to intensity, environmental flow, and the number and direction of outflow channels present.

5. Discussion and Conclusions

Upper troposphere outflow was examined for two eastern and central Pacific hurricanes in the 2014 season, Iselle and Julio. Greatest outflow magnitudes in both TCs were found located vertically between 150 and 200 hPa, in agreement with both *Emanuel and Rotunno* [2011], who found the majority of TC outflow focused below the tropopause, and *Molinari et al.* [2014], who found outflow maximum near 12 km altitude (near 200 hPa). As both TCs intensified, the maximum outflow magnitude moved radially inward toward the TC center. Outflow magnitude was largest during periods of intensification and smallest during periods of weakening, a pattern that was found in both storms. This relationship between increase in outflow magnitude and increase in TC intensity is in good agreement with many studies that previously identified such a relationship [e.g., *Sadler*, 1976; *Chen and Gray*, 1986; *Merrill*, 1988; *Molinari and Vollaro*, 1989; *Pfeffer and Challa*, 1992; *Wu and Emanuel*, 1994; *Frank and Ritchie*, 1999; *Hanley et al.*, 2001; *Kimball and Evans*, 2002; *Rappin et al.*, 2011]. The inward radial progression during intensification noted in both TCs is a result that has not received as much attention, but that agrees with the enhanced divergence (and subsequent mass evacuation from the core) arguments of *Molinari et al.* [1995] and *Grimes and Mercer* [2015]. Indeed, as was found by *Emanuel* [2012] and *Wang et al.* [2014], greater outflow provides a critical connection between the TC boundary layer and the upper troposphere environment. Thus, it is not surprising that both TCs strengthened as outflow increased closer to the storm center and thus closer to the ascending branch of the TC Carnot engine.

Both Iselle and Julio exhibited a single outflow channel during most of the intensification portion of their life cycles. This single, asymmetric outflow channel was found by *Merrill* [1988] to be a defining characteristic of many intensifying TCs. In Iselle, dual outflow channels were noted about 24 h before and after peak intensity, while Julio largely maintained a broad outflow channel throughout its life cycle. After maximum intensity, outflow in Iselle shifted from dual channels to a single outflow channel, along with an overall decline in magnitude of outflow for the remainder of the storm's life cycle. In Julio, outflow shifted from primarily equatorward to primarily poleward, along with an overall decline in outflow magnitude similar to Iselle. These changes in outflow direction in both storms were connected to the evolution of large-scale flow features, particularly the phasing of the subtropical jet ridges and troughs moving eastward north of both TCs. This connection between outflow direction and the larger-scale environment agrees well with the early studies of *Holland and Merrill* [1984]) and *Flatau and Stevens* [1989], as well as the recent results of *Molinari et al.* [2014], who noted that outflow channels are often responses to environmental factors (such as troughs or ridges) external to the TC. Shifts in meridional orientation (e.g., from equatorward to poleward) and in number of outflow channels (e.g., from one to two) did not appear to be related to TC intensity for these two storms.

Changes in outflow occurred in parallel with changes in inertial stability in both Iselle and Julio. Regions of highest (lowest) inertial stability were generally located clockwise (counterclockwise) from the maximum outflow. This pattern held during periods of both single and dual outflow channels and extends work from earlier studies that related outflow to inertial stability. For example, *Frankin et al*. [1996] noted that upper level outflow was strongest in Hurricane Gloria (1985) at radii where the inertial stability was weakest. In this study, azimuthal relationships between outflow and inertial stability were examined. *Rappin et al*. [2011] examined instantaneous relationships between inertial stability and outflow. In this study, the concurrent evolution in time of both was examined. Finally, *Li and Wang* [2012], as well as earlier work by *Black and Anthes* [1971], noted that inertial stability may play a role in the formation of asymmetries in upper troposphere outflow. Here highest (lowest) inertial stability was generally located clockwise (counterclockwise) from the maximum outflow throughout the life cycles of both Iselle and Julio, including for both equatorward and poleward directed outflows. The relationship even held during the period of dual outflow channels in Iselle. This means that the relationship is insensitive to changes in the synoptic-scale environmental flow, as poleward directed outflow tended to flow into the base of troughs to the northwest of the TCs and equatorward directed outflow tended to be associated with flow around ridges to the west of the TCs. This consistent spatial offset between outflow and inertial stability also suggests that the azimuthal position of outflow is related to azimuthal structure of inertial stability, similar to the suggestions of MV96 and *Molinari et al*. [2014]. Because outflow affects TC intensity, better understanding of potential dynamical and/or thermodynamical reasons for the azimuthal relationships consistently seen between outflow and inertial stability is a promising area of future work.

Acknowledgments

This work was partially sponsored by the ONR award N0001415WX01688 in support of the Tropical Cyclone Intensity Departmental Research Initiative. Atmospheric motion vector (AMV) observations were provided courtesy of the University of Wisconsin Cooperative Institute for Meteorological Satellite Studies, available at http://tropic.ssec.wisc.edu/archive/. Model analyses were provided courtesy of the Naval Research Laboratory Marine Meteorology Division, Monterey, CA, through the U.S. Global Ocean Data Assimilation Experiment, available at http://www.usgodae.org/. Dropsonde observations were provided courtesy of the NOAA Atlantic Oceanographic and Meteorological Laboratory (AOML), available at http://www.aoml.noaa.gov/hrd/Storm_pages/iselle2014/mission.html. The authors thank the anonymous reviewers for their helpful comments to improve the manuscript.

References

Archambault, H. M., L. F. Bosart, D. Keyser, and J. M. Cordeira (2013), A climatological analysis of the extratropical flow response to recurving Western North Pacific tropical cyclones, *Mon. Weather Rev.*, *141*, 2325–2346.

Black, P. G., and R. A. Anthes (1971), On the asymmetric structure of the tropical cyclone outflow layer, *J. Atmos. Sci.*, *28*, 1348–1366.

Bormann, N., K. Salonen, C. Peubey, T. McNally, and C. Lupu (2012), An overview of the status of the operational assimilation of AMVs at ECMWF, paper presented at 11th Int. Wind Workshop, Int. Working Winds Group Auckland, New Zealand, 4:2.

Bosart, L. F., and D. B. Dean (1991), The Agnes rainstorm of June 1972: Surface feature evolution culminating in inland storm redevelopment, *Weather Forecast.*, *6*(4), 515–537.

Chavas, D. R., and K. Emanuel (2014), Equilibrium tropical cyclone size in an idealized state of axisymmetric radiative–convective equilibrium, *J. Atmos. Sci.*, *71*(5), 1663–1680.

Chen, L., and W. M. Gray (1986), Global view of the upper level outflow patterns associated with tropical cyclone intensity change during FGGE, *Dep. of Atmos. Sci. Paper No. 392*, 126, Colorado State Univ., Fort Collins, Colo.

Corbosiero, K. L., and J. Molinari (2003), The relationship between storm motion, vertical wind shear, and convective asymmetries in tropical cyclones, *J. Atmos. Sci.*, *60*(2), 366–376.

Cotton, J., and M. Forsythe (2012), AMVs at the Met Office: Activities to improve their impact in NWP, paper presented at 11th Int. Wind Workshop, Int. Working Winds Group, Auckland, New Zealand, 4:3.

Cress, A. (2012), Recent progress in using satellite winds at the German Weather Service, presented at *11th Int. Wind Workshop*, Int. Working Winds Group, Auckland, New Zealand, 4:4.

Emanuel, K. (2010), Tropical cyclone activity downscaled from NOAA-CIRES reanalysis, 1908–1958, *J. Adv. Model. Earth Syst.*, *2*, 1, doi:10.3894/james.2010.2.1.

Emanuel, K. (2012), Self-stratification of tropical cyclone outflow. Part II: Implications for storm intensification, *J. Atmos. Sci.*, *69*(3), 988–996.

Emanuel, K. A. (1986), An air-sea interaction theory for tropical cyclones. Part I: Steady-state maintenance, *J. Atmos. Sci.*, *43*(6), 585–605.

Emanuel, K., and R. Rotunno (2011), Self-stratification of tropical cyclone outflow. Part I: Implications for storm structure, *J. Atmos. Sci.*, *68*(10), 2236–2249, doi:10.1175/jas-d-10-05024.1.

Emanuel, K., S. Solomon, D. Folini, S. Davis, and C. Cagnazzo (2013), Influence of tropical tropopause layer cooling on Atlantic hurricane activity, *J. Clim.*, *26*(7), 2288–2301, doi:10.1175/jcli-d-12-00242.1.

Ferreira, R. N., and W. H. Schubert (1999), The role of tropical cyclones in the formation of tropical upper-tropospheric troughs, *J. Atmos. Sci.*, *56*(16), 2891–2907.

Flatau, M., and D. E. Stevens (1989), Barotropic and inertial instabilities in the hurricane outflow layer, *Geophys. Astrophys. Fluid Dyn.*, *47*(1–4), 1–18.

Frank, W. M., and E. A. Ritchie (1999), Effects of environmental flow upon tropical cyclone structure, *Mon. Weather Rev.*, *127*(9), 2044–2061.

Franklin, J. L., S. J. Lord, S. E. Feuer, and F. D. Marks Jr. (1993), The kinematic structure of Hurricane Gloria (1985) determined from nested analyses of dropwindsonde and Doppler radar data, *Mon. Weather Rev.*, *121*, 2433–2451.

Franklin, J. L., S. Feuer, J. Kaplin, and S. D. Aberson (1996), Tropical cyclone motion and surrounding flow relationships: Searching for beta gyres in Omega dropwindsonde datasets, *Mon. Weather Rev.*, *124*, 64–84.

Grams, C. M., S. C. Jones, C. A. Davis, P. A. Harr, and M. Weissmann (2013), The impact of Typhoon Jangmi (2008) on the midlatitude flow. Part I: Upper-level ridge building and modification of the jet, *Q. J. R. Meteorol. Soc.*, *139*(677), 2148–2164.

Grimes, A., and A. E. Mercer (2015), Synoptic-scale precursors to tropical cyclone rapid intensification in the Atlantic basin, *Adv. Meteorol.*, *2015*, 1–16, doi:10.1155/2015/814043.

Hack, J. J., and W. H. Schubert (1986), Nonlinear response of atmospheric vortices to heating by organized cumulus convection, *J. Atmos. Sci.*, *43*(15), 1559–1573.

Hanley, D., J. Molinari, and D. Keyser (2001), A composite study of the interactions between tropical cyclones and upper-tropospheric troughs, *Mon. Weather Rev.*, *129*(10), 2570–2584.

Harr, P. A., and R. L. Elsberry (2000), Extratropical transition of tropical cyclones over the Western North Pacific. Part I: Evolution of structural characteristics during the transition process, *Mon. Weather Rev.*, *128*(8), 2613–2633.
Harr, P. A., D. Anwender, and S. C. Jones (2008), Predictability associated with the downstream impacts of the extratropical transition of tropical cyclones: Methodology and a case study of Typhoon Nabi (2005), *Mon. Weather Rev.*, *136*(9), 3205–3225, doi:10.1175/2008mwr2248.1.
Henderson, J. M., G. M. Lackmann, and J. R. Gyakum (1999), An analysis of Hurricane Opal's forecast track errors using quasigeostrophic potential vorticity inversion, *Mon. Weather Rev.*, *127*(3), 292–307.
Hogan, T., et al. (2014), The Navy Global Environmental Model, *Oceanography*, *27*(3), 116–125, doi:10.5670/oceanog.2014.73.
Holland, G. J., and R. T. Merrill (1984), On the dynamics of tropical cyclone structural changes, *Q. J. R. Meteorol. Soc.*, *110*(465), 723–745.
Kimball, S. K., and J. L. Evans (2002), Idealized numerical simulations of hurricane–trough interaction, *Mon. Weather Rev.*, *130*(9), 2210–2227.
Kimberlain, T. B. (2014), Hurricane Iselle. National Hurricane Center tropical cyclone report. [Available at http://www.nhc.noaa.gov/data/tcr/ep102014_iselle.pdf, NOAA National Hurricane Center, 13 pp.]
Li, Q., and Y. Wang (2012), Formation and quasi-periodic behavior of outer spiral rainbands in a numerically simulated tropical cyclone, *J. Atmos. Sci.*, *69*, 997–1020.
Menzel, W. P. (2001), Cloud tracking with satellite imagery: From the pioneering work of Ted Fujita to the present, *Bull. Am. Meteorol. Soc.*, *82*(1), 33–47.
Merrill, R. T. (1988), Characteristics of the upper-tropospheric environmental flow around hurricanes, *J. Atmos. Sci.*, *45*(11), 1665–1677.
Merrill, R. T., and C. S. Velden (1996), A three-dimensional analysis of the outflow layer of Supertyphoon Flo (1990), *Mon. Weather Rev.*, *124*(1), 47–63.
Molinari, J., and D. Vollaro (1989), External influences on hurricane intensity. Part I: Outflow layer eddy angular momentum fluxes, *J. Atmos. Sci.*, *46*(8), 1093–1105.
Molinari, J., and D. Vollaro (2014), Symmetric instability in the outflow layer of a major hurricane, *J. Atmos. Sci.*, *71*(10), 3739–3746, doi:10.1175/jas-d-14-0117.1.
Molinari, J., S. Skubis, and D. Vollaro (1995), External influences on hurricane intensity. Part III: Potential vorticity structure, *J. Atmos. Sci.*, *52*(20), 3593–3606.
Molinari, J., P. Duran, and D. Vollaro (2014), Low Richardson number in the tropical cyclone outflow layer, *J. Atmos. Sci.*, *71*(9), 3164–3179.
Montgomery, M. T., and R. K. Smith (2014), Paradigms for tropical cyclone intensification, *Aust. Meteorol. Oceanogr. J.*, *64*, 37–66.
Mrowiec, A. A., S. T. Garner, and O. M. Pauluis (2011), Axisymmetric hurricane in a dry atmosphere: Theoretical framework and numerical experiments, *J. Atmos. Sci.*, *68*(8), 1607–1619.
Nieman, S. J., W. P. Menzel, C. M. Hayden, D. Gray, S. T. Wanzong, C. S. Velden, and J. Daniels (1997), Fully automated cloud-drift winds in NESDIS operations, *Bull. Am. Meteorol. Soc.*, *78*(6), 1121–1133.
Pauley, P., N. Baker, R. Langland, L. Xu, C. Velden, and M. Forsythe (2012), The impact of satellite atmospheric motion vectors in the U.S. Navy Global Data Assimilation System: The superob procedure, presented at 11th Int. Wind Workshop, Int. Working Winds Group, Auckland, New Zealand, 4:10.
Peirano, C. M., K. L. Corbosiero, and B. H. Tang (2016), Revisiting trough interactions and tropical cyclone intensity change, *Geophys. Res. Lett.*, *43*, 5509–5515, doi:10.1002/2016GL069040.
Pfeffer, R. L., and M. Challa (1992), The role of environmental asymmetries in Atlantic hurricane formation, *J. Atmos. Sci.*, *49*(12), 1051–1059.
Ramsay, H. A. (2013), The effects of imposed stratospheric cooling on the maximum intensity of tropical cyclones in axisymmetric radiative–convective equilibrium, *J. Clim.*, *26*(24), 9977–9985.
Rappin, E. D., M. C. Morgan, and G. J. Tripoli (2011), The impact of outflow environment on tropical cyclone intensification and structure, *J. Atmos. Sci.*, *68*(2), 177–194.
Rotunno, R., and K. A. Emanuel (1987), An air–sea interaction theory for tropical cyclones. Part II: Evolutionary study using a nonhydrostatic axisymmetric numerical model, *J. Atmos. Sci.*, *44*(3), 542–561.
Rozoff, C. M., D. S. Nolan, J. P. Kossin, F. Zhang, and J. Fang (2012), The roles of an expanding wind field and inertial stability in tropical cyclone secondary eyewall formation, *J. Atmos. Sci.*, *69*(9), 2621–2643.
Sadler, J. C. (1976), Tropical cyclone initiation by the tropical upper tropospheric trough. *Dep. of Meteorology Paper No. 75-02*, 103, Univ. of Hawaii, Honolulu, Hawaii.
Salonen, K., J. Cotton, N. Bormann, and M. Forsythe (2015), Characterizing AMV height-assignment error by comparing best-fit pressure statistics from the met office and ECMWF data assimilation systems, *J. Appl. Meteorol. Climatol.*, *54*(1), 225–242.
Schmetz, J., K. Holmlund, J. Hoffman, B. Strauss, B. Mason, V. Gaertner, A. Koch, and L. V. D. Berg (1993), Operational cloud-motion winds from meteosat infrared images, *J. Appl. Meteorol.*, *32*(7), 1206–1225.
Schubert, W. H., and J. J. Hack (1982), Inertial stability and tropical cyclone development, *J. Atmos. Sci.*, *39*(8), 1687–1697.
Sears, J., and C. S. Velden (2014), Investigating the role of the upper-levels in tropical cyclone genesis, *Trop. Cyclone Res. Rev.*, *3*(2), 91–110, doi:10.6057/2014TCRR02.03.
Shapiro, L. J., and H. E. Willoughby (1982), The response of balanced hurricanes to local sources of heat and momentum, *J. Atmos. Sci.*, *39*(2), 378–394.
Shapiro, L. J., and M. T. Montgomery (1993), A three-dimensional balance theory for rapidly rotating vortices, *J. Atmos. Sci.*, *50*, 3322–3335.
Stewart, S. R. (2015), Hurricane Julio. National Hurricane Center tropical cyclone report. [Available at http://www.nhc.noaa.gov/data/tcr/EP102014_Julio.pdf, NOAA National Hurricane Center, 16 pp.]
Su, X., J. Derber, and J. Jung (2012), Recent work on satellite atmospheric motion vectors in the NCEP data assimilation system, presented at 11th Int. Wind Workshop, Int. Working Winds Group, Auckland, New Zealand, 4:13.
Torn, R. D. (2010), Diagnosis of the downstream ridging associated with extratropical transition using short-term ensemble forecasts, *J. Atmos. Sci.*, *67*(3), 817–833.
Torn, R. D., J. S. Whitaker, P. Pegion, T. M. Hamill, and G. J. Hakim (2015), Diagnosis of the source of GFS medium-range track errors in Hurricane Sandy (2012), *Mon. Weather Rev.*, *143*(1), 132–152.
Velden, C., J. Daniels, D. Stettner, D. Santek, J. Key, J. Dunion, K. Holmlund, G. Dengel, W. Bresky, and P. Menzel (2005), Recent innovations in deriving tropospheric winds from meteorological satellites, *Bull. Am. Meteorol. Soc.*, *86*(2), 205–223, doi:10.1175/bams-86-2-205.
Wang, S., S. J. Camargo, A. H. Sobel, and L. M. Polvani (2014), Impact of the tropopause temperature on the intensity of tropical cyclones: An idealized study using a mesoscale model, *J. Atmos. Sci.*, *71*(11), 4333–4348.
Wu, C.-C., and K. A. Emanuel (1993), Interaction of a baroclinic vortex with background shear: Application to hurricane movement, *J. Atmos. Sci.*, *50*(1), 62–76.
Wu, C.-C., and K. A. Emanuel (1994), On hurricane outflow structure, *J. Atmos. Sci.*, *51*(13), 1995–2003.
Wu, C.-C., and Y. Kurihara (1996), A numerical study of the feedback mechanisms of hurricane–environment interaction on hurricane movement from the potential vorticity perspective, *J. Atmos. Sci.*, *53*(15), 2264–2282.